Prepared for submission to JCAP
YITP-SB-16-NN

Distinguishing Dark Matter Models Using Annual Modulation

Samuel J. Witte,[a,b] **Vera Gluscevic,**[c] **and Samuel D. McDermott**[d]

[a]University of California, Los Angeles, Department of Physics and Astronomy, Los Angeles, CA 90095
[b]Fermi National Accelerator Laboratory, Center for Particle Astrophysics, Batavia, IL 60510
[c]School of Natural Sciences, Institute for Advanced Study, Einstein Drive, Princeton NJ 08540, USA
[d]C. N. Yang Institute for Theoretical Physics, Stony Brook, NY, USA

Abstract. In the event of a putative signal in future direct dark matter experiments, properly identifying the underlying dark matter-nuclei interaction promises to be a challenging task. Dark matter models with different dependencies on the momentum transfer produce qualitatively different nuclear recoil spectrum, and thus their signatures could potentially be disentangled should a significant number of events be observed simultaneously in various target nuclei. Interactions with identical momentum dependence (*e.g.* the spin-independent and anapole interaction), however, are unlikely to be identified using information on the nuclear recoil spectrum alone. The observed degeneracy between such models may be partially broken should interactions have different dependencies on the dark matter velocity, as this produces a qualitatively different time dependence of the scattering rate. Here, we investigate the extent to which including information on both the nuclear recoil energy and the time of observed events in the analysis of future direct detection data can be used to break model degeneracies. We show that including information on the annual modulation of the rate may significantly enhance the distinguishability of dark matter models with nearly degenerate recoil spectra, but only with exposures beyond what is produce in Generation 2 direct detection experiments.

Contents

1 Introduction

A vast array of independent astrophysical and cosmological observations testifies to the existence of a non-baryonic form of matter in the universe. This so-called dark matter (DM) is the dominant source of the gravitational potential wells that dictate the dynamics and structure of the universe. Despite experimental efforts on multiple fronts, including a direct detection program that has now been mature for several decades, efforts to elucidate potential non-gravitational interactions of dark matter with Standard Model particles have been unsuccessful.

As the next–generation direct detection experiments that incorporate increasingly sensitive detection technologies come online, they will start to probe the final portions of DM parameter space before encountering the irreducible neutrino backgrounds [1–10]. Generation 2 (G2) experiments that are currently taking data (see e.g. [2]) may well be on the cusp of important discoveries, as many interesting theories of DM predict scattering cross sections that live in these portions of paramters space. For example, heavy $SU(2)$–doublet and –triplet fermions, such as the Higgsinos and the wino of supersymmetry, are expected to have cross sections of order $\sigma_{\rm SI} \sim \mathcal{O}(\text{few} \times 10^{-48})\,\text{cm}^2$ (just about an order of magnitude below the current limits []`Sam, can you add a good citation?`, fixed by their Standard Model gauge quantum numbers alone [11–13], while a heavy $SU(2)$-singlet fermion, like the bino, is around an order of magnitude lower depending on its coannihilation partner [14]. Models with kinematically suppressed tree–level scattering may also be embedded in more complete dark sectors that have loop–level cross sections in this same range [15–18].

Because so many theories can be accommodated in the parameter space that will be imminently probed by a variety of experiments, it is timely to plan for the science opportunities associated with the first detection of DM particles. Most notably, in case of a confirmed detection,

understanding the high–energy dark sector dynamics will solely rely on examining low–energy recoils of detector elements and solving the "inverse problem" to identify the right underlying description of DM–baryon interactions from the experimental measurements. On the other hand, all the information about the dark sector interactions accessible to these measurements is contained within the coefficients of the "effective field theory of dark matter direct detection" [19, 20]. This effective description also captures the nontrivial nuclear physics induced by some of the best–motivated UV–complete theories of dark matter [21, 22] through an exhaustible list of dark matter-nuclei interactions. It thus provides a systematic framework for classifying and describing a wide variety of DM theories, and we will utilize it in this work.

However, due to Poisson noise and degeneracies in the shape of the recoil spectra amongst different interactions, DM model selection, and distinguishing amongst different effective descriptions has been shown to present a difficult task in practice, for a single target material. Recent studies have shown that discriminating between interactions is possible only for strong signals (with hundreds of observed recoil events), and only when measurements on targets with sufficiently diverse nuclear physics characteristics are jointly analyzed [22]. Thus, using energy spectra to break degeneracies in the dark matter modeling space crucially relies on "complementary" nuclear physics characteristics of available target materials [8, 22–28], but this alone does not guarantee successful model selection [25].

On the other hand, almost since the dawn of direct–detection–related DM studies, the motion of the Earth relative to DM bound in the galactic halo has been predicted to provide a distinctive DM signature [29–34] through characteristic annual modulation of the expected event rate of nuclear recoils. Recent work [35, 36] pointed out that non–standard interaction cross sections containing a non–factorizable velocity dependence could produce a modulation signal that is unique to each target element. More generally, a non–trivial velocity dependence in the cross section effectively changes the velocity integral that governs the total event rate in any given experiment, and produces a characteristic modulation signal. It may thus be expected that interaction models that differ solely by the power of velocity of their corresponding cross sections may differ by the phase and/or amplitude of the annual modulation signal they display.

Motivated by this argument, here we propose that analysis of time dependence of scattering events can help discriminate between interaction models whose recoil energy spectra are otherwise degenerate on a single target material. Using the method of [22], we evaluate the enhancement in prospects for accurate model selection when the annual modulation signal is analyzed in combination with recoil–energy measurements in the future generation direct detection experiments.

In Sec. 2 we review the calculation of the direct detection scattering rate and discuss how direct detection observables differ depending on the momentum and velocity dependence of the differential cross section. Sec. 3 summarizes the models and experiments that we consider in this paper, and introduces the statistical analysis we apply in order to determine the extent to which future direct detection experiments can properly identify the underlying dark matter model. Results are presented for various future generation experiments in Sec. 4. We conclude in Sec. 5.

2 Scattering in Direct Detection Experiments

2.1 Direct Detection Observables

The key measurement of most direct detection experiments is the nuclear recoil energy spectrum—the number count of nuclear recoil events per recoil energy E_R, per unit time t, per unit target mass,

$$\frac{dR}{dE_R dt}(E_R, t) = \frac{\rho_\chi}{m_T m_\chi} \int_{v_{\rm min}}^{v_{\rm esc,lab}} v f(\mathbf{v}, t) \frac{d\sigma_T}{dE_R}(E_R, v) d^3 v, \tag{2.1}$$

where ρ_χ is the local DM density; m_χ is the DM particle mass; m_T is the mass of the target nucleus T; $\mathbf{v}$ is DM velocity vector of magnitude v (in the lab frame); $f(\mathbf{v}, t)$ is the observed DM velocity distribution; $d\sigma_T/dE_R = m_T \sigma_T / 2\mu_T^2 v^2$ is the differential cross section for DM scattering off a nucleus T; and $\mu_T \equiv \frac{m_T m_\chi}{m_T + m_\chi}$ is the reduced mass of the DM particle and the target nucleus. Integration limits are the minimum velocity a DM particle requires in order to impart a nuclear recoil of energy E_R, which for elastic scattering[1] is given by $v_{\rm min} = \sqrt{m_T E_R / 2\mu_T^2}$, and the escape velocity from the Galactic halo in the lab frame, $v_{\rm esc,lab}$.

The differential rate in Eq. (2.1) is determined by the experimental setup, the DM astrophysical and particle properties, the nuclear properties of the target material, and the DM–nucleus interaction.[2] For the purposes of this study, we set the astrophysical parameters to the following values [37, 38]: $\rho_\chi = 0.3$ GeV/cm^3; $v_{\rm esc} = 533$ km/sec (in the Galactic frame), and assume that $f(\mathbf{v})$ is a Maxwellian distribution in the Galactic frame, with a rms speed of 155 km/sec and a mean speed equal to the Sun's rotational velocity around the Galactic center, $v_{\rm lag} = 220$ km/sec.

The underlying particle physics interaction determines the calculation of the recoil rate through the differential scattering cross section $d\sigma_T/dE_R$ [21, 22]. This quantity has a normalization (in units of cm^2) which is a free parameter of the model. Different interactions display different functional dependences on E_R and v, as discussed in detail in Refs. [21, 22] and summarized below in Sec. 2.2.

The total rate R of nuclear recoil events (per unit time and unit mass) is given by the integral of the differential rate within the nuclear–recoil energy window $\mathcal{E}$ of a given experiment[3], $R(t) = \int_{\mathcal{E}} \frac{dR}{dE_R dt} dE_R$. In turn, the total expected number of events $\langle N_{\rm tot} \rangle$ for a fiducial target mass $\mathcal{M}_{\rm fid}$, in experiment that started observation at a time t_1 and ended at a time t_2, is

$$\langle N_{\rm tot} \rangle = \mathcal{M}_{\rm fid} \int_{t_1}^{t_2} \int_{\mathcal{E}} \frac{dR}{dE_R dt}(E_R, t)\, dE_R\, dt. \tag{2.2}$$

[1] We restrict our attention in this work to dark matter-nuclei elastic scattering, and defer the subject of proper identification of scattering kinematics to later work.

[2] Throughout this paper we use T to denote the nuclear target and N to denote a nucleon, either neutron n or proton p

[3] For simplicity, we assume unit efficiency of detection within the analysis window, and rescale individual experimental exposures to take this assumption into account when choosing experimental parameters to represent the capabilities of G2 experiments.

2.2 Momentum and Velocity Dependence

Traditional focus on the two standard scattering cases: spin–independent (SI) and spin–dependent (SD) scattering (the former involves coherent contributions from the entire nucleus, resulting in a cross section that scales quadratically with nucleon number, while the latter scales with the total nuclear spin) obscures the richness of phenomenologies accessible to direct detection experiments, which can arise when the two standard interactions are suppressed [] Sam, do you have a good ref for this?. Here we summarize the effective field theory that catalogues all possible energy and velocity dependencies of the cross section, and thus delineates the modeling space for interactions probed by these experiments in most general terms. In the Sec. 3.1, we highlight several well–motivated examples of interesting scattering models which we use in this work to examine the extent to which including time information can enhance identification of the underlying model.

The effective field theory of DM direct detection [19, 20] relies on an expansion in two small kinematic variables: $|\vec{q}|/m_N$, where $\vec{q}$ is the change in momentum of the DM particle during the scattering, and $|\vec{v}_\perp|$ is the orthogonal component of the relative velocity of the initial–state particles. For an incoming (outgoing) DM three–momentum $\vec{p}(\vec{p}')$, incoming (outgoing) nuclear three–momentum $\vec{k}$ $(\vec{k}')$, and a reduced mass $\mu_{\chi N} \equiv m_\chi m_N/(m_\chi + m_N)$, these factors are $\vec{q} = \vec{p}' - \vec{p} = \vec{k} - \vec{k}'$, and $\vec{v}_\perp = \frac{\vec{p}}{m_\chi} - \frac{\vec{k}}{m_N} + \frac{\vec{q}}{2\mu_{\chi N}}$, respectively. The momentum transfer is directly related to the nuclear recoil energy as $\vec{q}^2 = 2m_T E_R$.

These expansion parameters are of the same order of magnitude, but it is important to note that they manifest differently in the observables of the scattering events (see *e.g.* Figs. 2 and 3 of **??**). In particular, terms that enter at higher order in $|\vec{q}|/m_N$ deliver a vanishing event rate at both small and large momentum transfer (or recoil–energy), with a maximum rate at some intermediate recoil energy, producing a "turnover feature" in the recoil–energy spectrum. Light mediator models can alternatively contain factors of $m_N/|\vec{q}|$, producing a steep enhancement of the recoil spectra at low values of E_R. On the other hand, higher–order terms in $|\vec{v}_\perp|$ produce rates that monotonically decrease with energy and are quantitatively similar to the standard SI or SD interaction case.

As was demonstrated by Ref. [22], the interaction models that feature different momentum dependence can be differentiated from each other using a single nuclear target, provided a sufficiently large exposure and event number counts; however, the latter class of models—those that differ only by the power of velocity dependence—are far more difficult to disentangle, leaving substantial degeneracy between well–motivated interaction models. In the following, we develop an intuition for how this degeneracy might be overcome, using annual modulation and time dependence of the scattering rate.

2.3 Time Dependendence

In Eq. (2.1), the differential rate of nuclear recoils is explicitly denoted as depending on time, which arises as a consequence of the Earth's harmonic motion around the Sun. This "annual modulation" of the DM particle "wind", as observed in the lab frame, is additionally affected by "gravitational focusing" of DM particles in the Sun's potential well [39–42]. Overall, these effects are expected to give rise to an energy–dependent modulation of the total nuclear recoil rate in direct detection experiments.

To illustrate the effects of annual modulation as well as the previously discussed energy and velocity dependence of different interactions, Fig. 1 compares the energy spectra (left column)

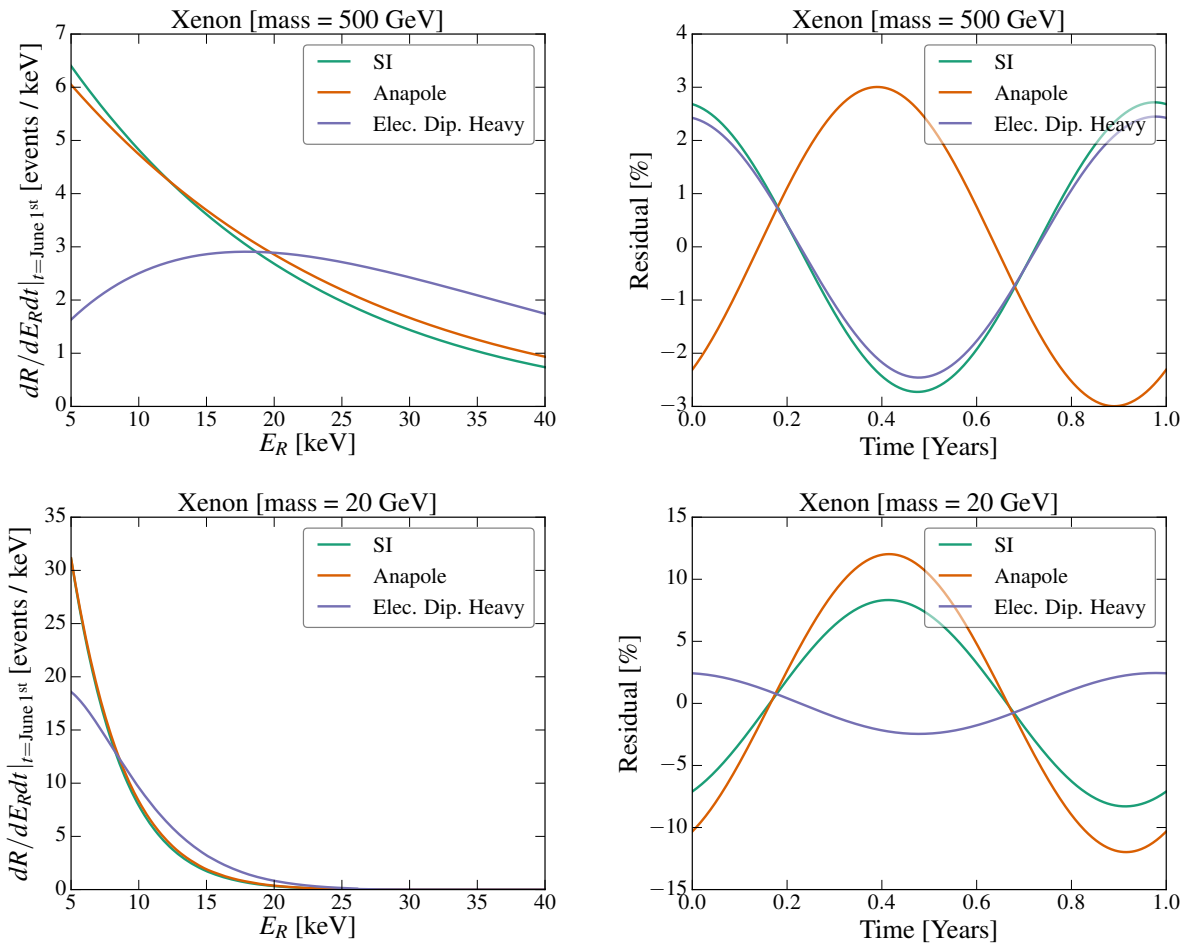

Figure 1. Comparison of the nuclear–recoil energy spectra (left column) and annual modulation signals (right column) between the SI (blue), anapole (black), and ED-heavy (green) interaction models on a xenon target, where the cross sections have been normalized to the current LUX 90% CL upper limits [43]. *Left:* Differential rate evaluated at June 1^{st} as a function recoil energy for a 500 GeV (top) and 20 GeV (bottom) DM particle. *Right:* Residual event rate (fractional deviation in the total event rate) as a function of time, for a 500 GeV (top) and 20 GeV (bottom) DM particle.

and time dependencies of the total expected event rates (right column) under several interaction scenarios: the standard SI interaction, anapole, and heavy–mediator electric dipole (ED–heavy) interaction (see Sec. 3.1 for a more detailed definition of the models). The top (bottom) panels of Fig. 1 correspond to a 500 (20) GeV DM particle. Instead of showing the differential rate as a function of time in the right–hand panels we show the residuals, defined as the fractional deviation from the time–averaged energy–integrated rate. Note, for example, that the energy spectra for the SI and ED–heavy interactions are distinct in a way that the SI and anapole interactions are not; thus, discerning the SI and anapole hypotheses using the energy spectrum alone is quite challenging, given even the most optimistic expectations for the Poisson noise [22].

However, the annual–modulation signatures of SI and anapole models can be very different, owing to a non–trivial ($\sim |\vec{v}_\perp|^2$) velocity dependence of the cross section of the latter model. This in turn leads to different velocity integrals in Eq. (2.1), and through the effects of annual rate modulation, to different time dependence of the total event rates in the two models. For large enough DM mass, this can produce a nearly *opposite modulation phase* between the standard SI scenario and the anapole case! Furthermore, differential cross sections which contain multiple non–negligible terms with different velocity dependences can produce annual modulation signals entirely unique to a given target element [35, 36]. The time variation of the rate, and thus the differences between the annual modulation produced by these models, is typically expected to be small – on the order of a few percent. Nonetheless, we will show in the following that this small difference in the characteristic time dependence of the rate for different models can be used to supplement the information contained in the energy spectrum and substantially aid the process of model selection on a single target with future experiments. In the following analysis, we incorporate calculations of the annual modulation signal and the effect of gravitational focusing following the procedure of [44].

3 Distinguishing Scattering Models

Our approach, outlined below, follows that of Ref. [22]. We being in Sec. 3.1 by identifying various realistic models which produce dark matter-nuclei interactions with a similar dependence on the momentum transfer but different dependencies on the dark matter velocity (*i.e.* models with nearly degenerate recoil spectra but qualitatively different annual modulation). Assuming a particular DM model and mass, we simulate events in future direct detection experiments assuming optimistically that the true cross section is at the current 90% CL. This procedure is repeated for many realizations in order to capture in the impact of Poisson noise on future data analyses (refer to Sec. 3.2 for specific details). We then perform a Bayesian model selection analysis between two models with nearly degenerate recoil spectrum but differing time dependence, in order to quantitatively assess the impact that including time information may potentially have on proper model identification. The details of this statistical procedure are outline in Sec. 3.3.

3.1 Summary of Models

In this section, we illustrate a generic model which can give rise to various dark matter-nuclei interactions that contain different dependencies on the momentum transfer and DM velocity. We emphasize that the discussion below is simply one illustration that gives rise to operators that we are interested in studying, and is by no means an exhaustive list of models which can lead to these types of interactions.

In order to assess the benefit from considering time dependence of the scattering signals in direct–detection analyses with future data, we focus on a subset of scattering models: a generic model of new physics, represented by a hidden $U(1)'$ that has several charged fermions X_i and a heavy gauge boson A'_μ with mass M that kinetically mixes with the Standard Model photon. At high energies, the Lagrangian contains

$$\mathcal{L} \supset -m_X \bar{X}_i X^i + i\bar{X}_i \not{\partial}_{ij} X^j - \frac{1}{2} M^2 A'_\mu A'^\mu - \frac{1}{4} F'_{\mu\nu} F'^{\mu\nu} - \frac{\epsilon}{2} F'_{\mu\nu} F^{\mu\nu} \,, \tag{3.1}$$

where $F_{\mu\nu}$ and $F'_{\mu\nu}$ are the field strength tensor of the photon and the heavy gauge boson, respectively (*i.e.* $F_{\mu\nu} \equiv \partial_\mu A_\nu - \partial_\mu A_\nu$). At low energies, the A'_μ and most X particles are integrated out. We assume a mass hierarchy that results in an electrically neutral fermion χ as the lightest degree of freedom in the dark sector. Because of the kinetic mixing, the state χ couples to the Standard Model nucleon current [21],

$$\mathcal{J}_\mu = \partial^\alpha F_{\alpha\mu} = e \sum_{n,p} \bar{N} \left(Q_N \frac{K_\mu}{2m_N} - \tilde{\mu}_N \frac{i\sigma_{\mu\nu} q^\nu}{2m_N} \right) N, \tag{3.2}$$

where $Q_{p(n)} = 1(0)$ are the nucleon charges in units of the electron charge e, $K_\mu/2 = (k_\mu + k'_\mu)/2$ is the average nucleon momentum, and $\tilde{\mu}_N = \frac{\text{magnetic moment}}{\text{nuclear magneton}}$ is the dimensionless magnetic moment of the nucleon.

The details of the masses and charges of the dark fermions X_i that constitute or couple to the dark matter χ will determine interaction that is measured in an experiment. We will use $\mathcal{O}^\mu_\chi$ to denote the Lorentz-vector fermion bilinear that couples to the current in Eq. (3.2). Because we assume χ is electromagnetically neutral, the possible $\mathcal{O}^\mu_\chi$ are [21, 22]

$$\mathcal{O}^\mu_{\chi,\text{Anapole}} = g^{\text{Anapole}} \bar{\chi} \gamma^\mu \gamma_5 \chi, \tag{3.3}$$

$$\mathcal{O}^\mu_{\chi,\text{MD}} = \frac{g^{\text{MD}}}{\Lambda} \bar{\chi} i\sigma^{\mu\nu} q_\nu \chi, \tag{3.4}$$

$$\mathcal{O}^\mu_{\chi,\text{ED}} = \frac{g^{\text{ED}}}{\Lambda} \bar{\chi} i\sigma^{\mu\nu} \gamma_5 q_\nu \chi. \tag{3.5}$$

Alternatively, if the mass of mediator is small relative to the characteristic scale of momentum transfer, the ED and MD interactions are described by the following operators:

$$\mathcal{O}^\mu_{\chi,\text{MD}} = g^{\text{MD}} \bar{\chi} i\sigma^{\mu\nu} \chi, \tag{3.6}$$

$$\mathcal{O}^\mu_{\chi,\text{ED}} = g^{\text{ED}} \bar{\chi} i\sigma^{\mu\nu} \gamma_5 \chi. \tag{3.7}$$

As stated above, the interaction operator for χ is determined by the dynamics of the X fermion(s). The anapole current in Eq. (3.6) will arise if charged $X^\pm$ states condense to form a neutral Majorana state χ [45]. The dipole currents form if an electromagnetically neutral X^0 couples to an electromagnetically charged pair of partner $X^\pm$ particles (of appropriate spin) [46]. The scale at which the charged X states are integrated out is Λ.

The simplicity of the model in Eq. (3.1) and the rich assortment of momentum and velocity dependence that appear in the associated EFT operators illustrates the generic nature of these interactions. We list the EFT classification of these operators in Tab. 1. (This is an abbreviated version of the more exhaustive table that appeared in [22], using results of [21, 22]). In this work, we will focus on differentiating dark matter-nuclei interactions that have the same momentum scaling but different velocity dependence.

3.2 Simulations

For our simulations, we consider interactions discussed in previous Section, and examine three test masses for DM particle: 20 GeV, 125 GeV, and 500 GeV. In all our simulations, we optimistically

Model name	Lagrangian	$\vec{q}$, v Dependence
SI	$\frac{g}{M^2}\bar{\chi}\chi\bar{N}N$	1
Anapole	$\frac{g}{M^2}\bar{\chi}\gamma^\mu\gamma_5\chi\,\mathcal{J}_\mu$	$v_\perp^2, \vec{q}^2/m_N^2$
Magnetic Dipole (Heavy)	$\frac{g}{\Lambda M^2}\bar{\chi}\sigma^{\mu\nu}\chi\,q_\nu\mathcal{J}_\mu$	$\frac{\vec{q}^4}{\Lambda^4} + \frac{\vec{q}^2 v_\perp^2}{\Lambda^2}, \vec{q}^4/\Lambda^4$
Electric Dipole (Heavy)	$\frac{g}{\Lambda M^2}\bar{\chi}\sigma^{\mu\nu}\gamma_5\chi\,q_\nu\mathcal{J}_\mu$	$\vec{q}^2/\Lambda^2$
Magnetic Dipole (Light)	$\frac{g}{\Lambda}\bar{\chi}\sigma^{\mu\nu}\chi F_{\mu\nu}$	$1 + \frac{v_\perp^2 m_N^2}{\vec{q}^2}$, 1
Electric Dipole (Light)	$\frac{g}{\Lambda}\bar{\chi}\sigma^{\mu\nu}\gamma_5\chi F_{\mu\nu}$	$m_N^2/\vec{q}^2$

Table 1. Selection of operators along with their EFT dependences, adapted from [22]. The labels 'Light' and 'Heavy' in the dipole models denote the magnitude of the mediator mass relative to the characteristic momentum transfer. The nucleon electromagnetic current $\mathcal{J}_\mu$ is defined in Eq. (3.2); the transverse velocity $v_\perp$ and three–momentum transfer $\vec{q}$ are defined in terms of the collision momenta (see Sec. 2.2); and Λ is a heavy mass or compositeness scale appearing in the dipole models. Terms in the third column that induce different nuclear responses, and thus require different form factors, are separated by a comma (see *e.g.* [20] for more details).

Label	A (Z)	Energy window [keVnr]	Exposure [kg-yr]
Xe	131 (54)	5-40	2000
Ge	73 (32)	0.3-100	100
F	19 (9)	3-100	606
Xe(x3)	131 (54)	5-40	6000
Xe(x10)	131 (54)	5-40	20 000
XeG3	131 (54)	5-40	40 000

Table 2. Mock experiments considered in this work. The efficiency and the fiducialization of the target mass are included in the exposure. The first group of experiments is chosen such to be representative of the reach of Gen2 experiments for Xe, Ge, and F. The exposure for Xe and Ge is chosen to agree with the projected exclusion curves for LZ and SuperCDMS presented in Ref. [6]. The second group of experiments is used to quantitatively assess the impact of including the timing information as a function of the exposure, i.e. the observed number of events.

set the cross section to be the value maximally allowed by LUX null results [43] [4]. Our initial analysis focuses on Gen2 experiments, specifically xenon, germanium, and fluorine based targets. Since fluorine experiments measure only the energy integrated rate, information on recoil energies of individual events are neglected in this case. The exposure and energy window of our mock experiments are summarized in Table 2. Throughout the analysis we assume unit detection efficiency

[4]We note that LUX currently produces the most constraining bounds on the models and masses of considered in this paper, although the constraint from PandaX-II is only marginally weaker [47].

Interaction /target	Xe	Ge	F
m_χ [GeV]	(20, 125, 500)	(20, 125, 500)	(20, 125, 500)
SI	(103, 99, 98)	(9, 4, 4)	(5, 1, 2)
Anapole	(103, 97, 96)	(11, 5, 5)	(36, 3, 3)
Mag. dip. heavy	(103, 89, 87)	(3, 4, 5)	(4, 1, 1)
Mag. dip. light	(103, 101, 101)	(34, 14, 14)	(86, 16, 15)
Elec. dip. heavy	(103, 91, 88)	(4, 4, 4)	(1, 0, 0)
Elec. dip. light	(103, 102, 101)	(61, 15, 14)	(40, 12, 12)

Table 3. Predicted number of events in Gen2 experiments for various interactions with xenon, germanium, and fluorine targets assuming a DM mass of (20 GeV, 125 GeV, and 500 GeV). The predicted numbers of events are calculated using a cross section set to the current 90% upper limits. Labels 'light' and 'heavy' denote the relative relation between the mediator mass and the characteristic scale of momentum transfer.

and zero backgrounds. In addition to the aforementioned, we also consider the potential reach of a Generation 3 (Gen3) xenon experiment, as well as various xenon experiments with exposures lying somewhere between Gen2 and Gen3 (the properties of which are summarized in Table 2). The predicted number of events in these mock experiments are shown in Table 3.

For each simulation, the observed number of events is obtained by randomly selecting from a Poisson distribution with a mean given by the predicted number of events calculated using Eq. (2.2). The recoil energy and time of each event is then obtained by applying a rejection sampling algorithm to the two-dimensional differential scattering rate.

3.3 Analysis method

Within the Bayesian inference framework, the probability that the data $\vec{X}$ assigns to a given model $\mathcal{M}_j$ is given by

$$P(\mathcal{M}_j) = \frac{\mathcal{E}_j(\vec{X}|\mathcal{M}_j)}{\sum_i \mathcal{E}_i(\vec{X}|\mathcal{M}_i)}\,, \tag{3.8}$$

where $\mathcal{E}(\vec{X}|\mathcal{M})$ is the evidence of model $\mathcal{M}$, defined by

$$\mathcal{E}(\vec{X}|\mathcal{M}) = \int d\Theta\, \mathcal{L}(\vec{X}|\Theta, \mathcal{M})\, p(\Theta, \mathcal{M})\,, \tag{3.9}$$

and is intuitively understood to be the factor required to normalize the posterior $\mathcal{P}$, *i.e.*

$$\mathcal{P}(\Theta|\vec{X}, \mathcal{M}) = \frac{\mathcal{L}(\vec{X}|\Theta, \mathcal{M})\, p(\Theta, \mathcal{M})}{\mathcal{E}(\vec{X}|\mathcal{M})}\,. \tag{3.10}$$

Here, $\mathcal{L}(\vec{X}|\Theta, \mathcal{M})$ is the likelihood, *i.e.* the probability of obtaining the data, given a particular model $\mathcal{M}$ and parameters Θ (for the purpose of this analysis $\Theta = \{m_\chi, \sigma_p\}$), and $p(\Theta, \mathcal{M})$ is the

prior. In order to remain as agnostic as possible, we take wide priors in both m_χ and σ_p[5]. In our analysis we use an unbinned extended likelihood function of the form

$$\mathcal{L}(\vec{X}|\Theta,\mathcal{M}) = \frac{\mu^N}{N!}\, e^{-\mu} \prod_{x_i \in \vec{X}} \frac{1}{\mu} \frac{dR}{dE_R dt}\bigg|_{E_R, t=x_i}, \tag{3.11}$$

where μ is the predicted number of events, N is the number of observed events, and the product runs over all the normalized differential rate evaluated at the E_R and t values of each observed event $x_i \equiv \{E_{R,i}\,,\, t_i\}$. When time or E_R information is neglected, the differential rate is implicitly understood to be averaged over that variable.

Our analysis proceeds as follows. We begin by simulating data for an experiment (or experiments) assuming a particular dark matter model, mass, and cross section (see Sec. 3.2). We then use PyMultiNest to reconstruct the posterior defined in Eq. (3.10), and subsequently calculate the evidence for various dark matter models [48, 49][6]. Once the evidence of various models has been computed, one can estimate the probability of successfully being able to identify the true model using Eq. (3.8). This procedure is then repeated for $\simeq \mathcal{O}(50)$ simulations to assess the variability in successful model identification arising from Poisson fluctuations. A model is said to be correctly identified if the probability determined using Eq. (3.8) is large. For the purpose of this paper, we define the boundary for successful model identification at $P \geq 90\%$. The primary quantity of interest for future direct detection experiments is then the fraction of simulations which lead to a successful model identification.

Instead of plotting the individual probabilities of each simulation, we apply kernel density estimation (KDE) with a Gaussian kernel to determine the distribution functions of these probabilities. For of the results listed in the following section, we plot the KDE distribution for each experimental combination both with and without time, and determine the fractional success rate by integrating the distribution above the 90% threshold.

4 Results

We begin by considering the extent to which including time information in the analysis of Gen2 experiments can assist in breaking degeneracy between the SI and anapole interactions. Specifically, in Fig. 2 we consider the probability of correctly identifying the anapole (left) and SI (right) interactions, assuming a putative signal is detected in either a xenon experiment (red) or in a combination of xenon, germanium, and fluorine experiments (purple). Analysis is shown for a 500 GeV dark matter particle (top), 125 GeV dark matter particle (middle), and a 20 GeV dark matter particle (bottom), including (solid) and neglecting (dashed) information on the modulation.

Consistent with the results of [22], we find that both models can be correctly identified in Gen2 experiments for a 20 GeV dark matter particle, but only if detections are made in both xenon and fluorine based experiments (note that Xe+Ge analyses do not break the degeneracy and have no model discrimination). Should detections be made in both xenon and fluorine experiments, time information would not be needed to differentiate the two models.

[5] Log priors are taken for both m_χ and σ_p, spanning $1 - 3000$ GeV in mass and 7 orders of magnitude in cross section.

[6] Multinest runs are performed with 2000 live points, an evidence tolerance of 0.1, and a sampling efficiency of 0.3.

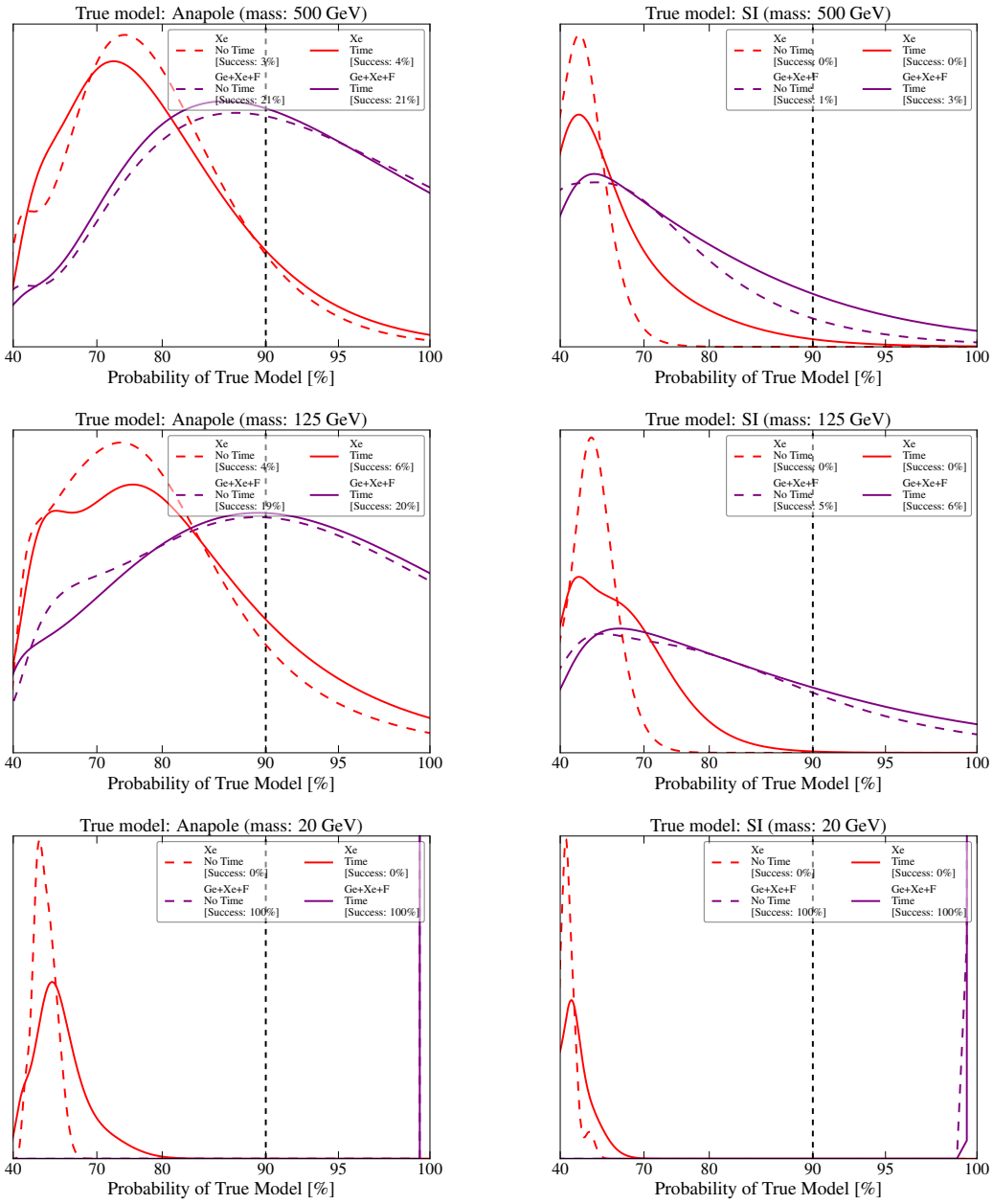

Figure 2. Model selection prospects with complimentary Gen2 targets. The normalized probability distribution functions for the probability of correctly identifying the true model are shown for the anapole (left) and SI (right) interactions, assuming a 500 GeV (top), 125 GeV (middle), and 20 GeV (bottom) dark matter particle. Results are shown for a xenon experiment (red), and a combined analysis of xenon, germanium, and fluorine experiments (purple), including (solid) and neglecting (dashed) information on the modulation of the rate. Success rate is defined to be the fraction of realizations which produce correct model identification at the level of $\geq 90\%$

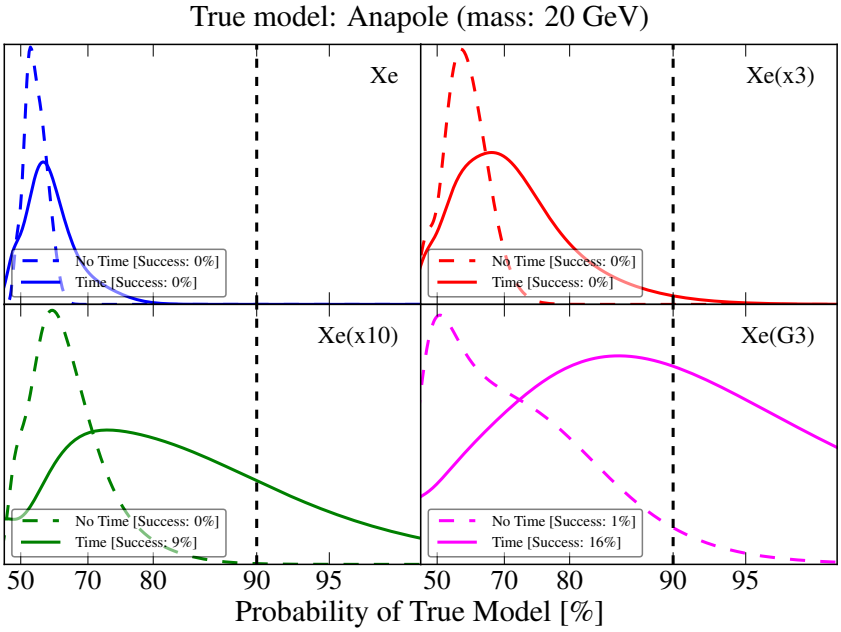

Figure 3. Model selection prospects for a single target (xenon), including (solid) and neglecting (dashed) information on the modulation of the rate. The normalized probability distribution functions are plotted for the probability associated with correcting identifying a 20 GeV dark matter particle scattering through the anapole interaction. Panels from left to right, top to bottom, correspond to exposure of 2 ton-years (blue), 6 ton-years (red), 20 ton-years (green), and 40 ton-years (magenta). Calculations are performed assuming the true cross section is sitting at the current 90% upper limit. Successful model identification, defined as having $\geq 90\%$ probability, are provided in the legend of each analysis.

Correct model identification is slightly more complicated for heavier dark matter candidates due to the reduced scattering rate in fluorine. For the anapole model, detection in Xe leads to a model discrimination of a few percent. If however, detections are made in xenon, germanium, and fluorine experiments, model selection could be as high as $\simeq 20\%$. Including time information only negligibly increases model selection in both cases. Model selection for the SI interaction is significantly reduced relative to that of the anapole interaction. Xenon experiments are completely unable to break this degeneracy if massive dark matter interacts through a SI interaction, regardless of whether or not time information is included in the analysis. Should detections be made in xenon, germanium, and fluorine experiments, correct model identification is still only at the level of a few percent. As with the anapole interaction, including time information in the analysis does not impact the ability of these experiments to correctly identify the underlying model.

Given that Gen2 experiments will optimistically detect $\simeq 100$ events for the SI and anapole interaction, it is not surprising that analyzing Gen2 data with time has a minimal effect on model selection (see *e.g.* Sec. 4 of [33] for an estimation of the number of events needed for phase discrimination). Perhaps the more interesting question is: how many events are needed before the inclusion of time information can significantly effect model selection? We address this question in the context of the breaking the SI and anapole degeneracy in xenon based experiments in Figs. 3-5.

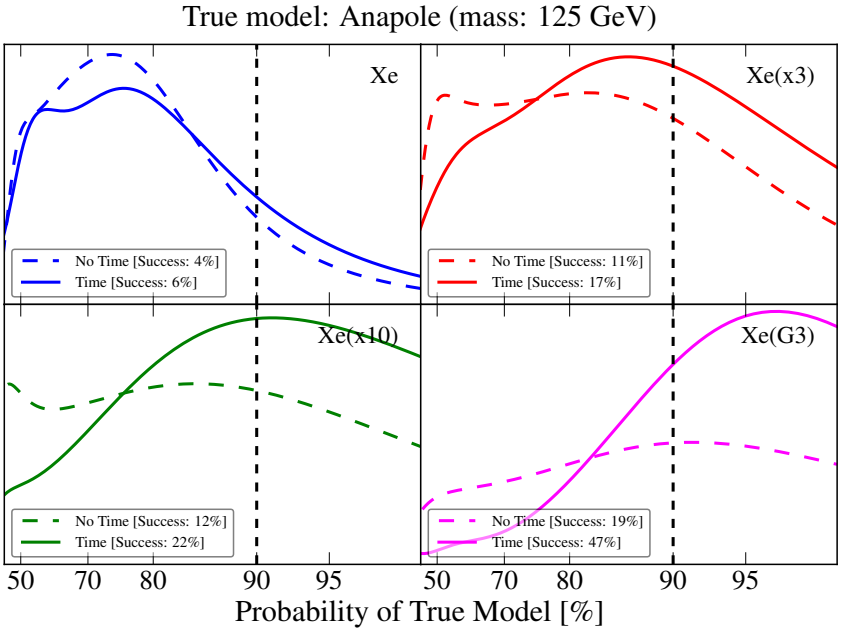

Figure 4. Same as Fig. 3 but for 125 GeV dark matter.

For 20, 125, and 500 GeV anapole dark matter, we plot the probability of correctly identifying the true model in a 2 ton-year (blue), 6 ton-year (red), 20 ton-year (green), and 40 ton-year (magenta) xenon experiment, neglecting (dashed) and including (solid) time information. Since results for the SI interaction are qualitatively similar to that of the anapole, we defer the SI analogues of Figs. 3-5 to Appendix A.

Fig. 1 clearly shows that the recoil spectrum observed in xenon arising from light anapole and SI dark matter is more degenerate than that of heavy anapole and SI dark matter. Unfortunately the phase of light dark matter is also degenerate for conventional velocity dependent cross sections (*i.e.* $d\sigma/dE_R \propto v^{-2}, v^0, v^2, ...$) [35, 36], suggesting that the inclusion of time information in the analysis may not be sufficient to fully differentiate these models. Indeed Fig. 3 shows that even in a Gen3 xenon experiment, the SI and anapole interaction can only be correctly identified in $\simeq 15\%$ of our simulations (assuming time is included). Perhaps surprisingly, however, is that the inclusion of time in the analysis improves model discrimination by $\simeq 15\%$. This improvement arises not from differences in the phase, but rather from the amplitude of the modulation, which as shown in Fig. 1 differs by $\simeq 5\%$.

As the dark matter mass increases the recoil spectrum become less degenerate, allowing for better model discrimination at fixed exposure. Additionally, heavier dark matter allows these experiments to probe regions of parameter space where the anapole and SI interaction are out of phase (see Fig. 1). Figs. 4 and 5 confirm that heavier dark matter candidates allow for better model discrimination of these models, particularly when time is included in the analysis. We emphasize that including time in the analysis can potentially improve model selection in Gen3 experiments by as much as $\simeq 30\%$ for heavy dark matter candidates, where the phase of these interactions may

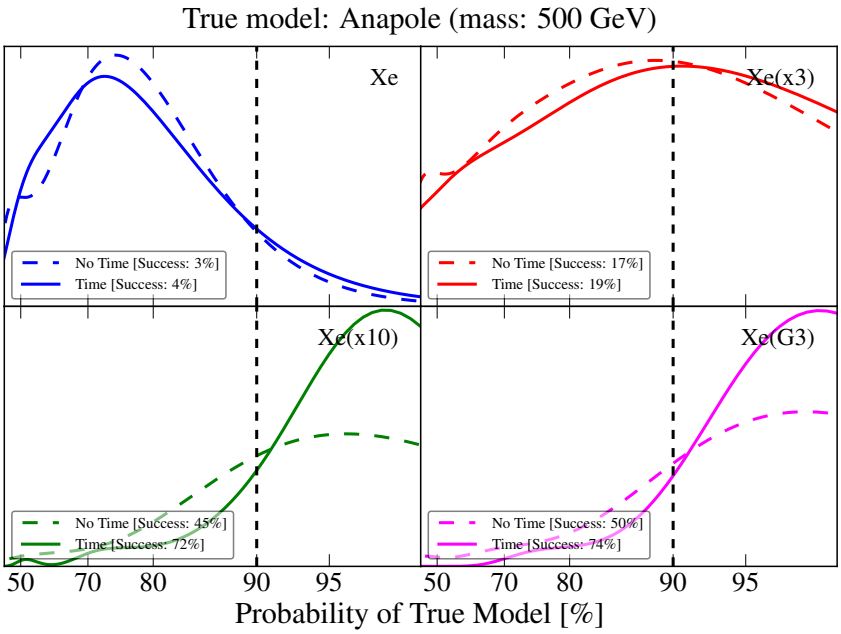

Figure 5. Same as Fig. 3 but for 500 GeV dark matter.

be misaligned by as much as $\simeq 5$ months. Despite this improvement, Gen3 experiments will likely also need to exploit target complimentarily to in order to fully break the SI-anapole degeneracy.

To briefly summarize the conclusions of Figs. 3-5, including time information in the analysis of future xenon direct detection experiments begins to significantly enhance model selection after $\simeq \mathcal{O}(1000)$ ($\mathcal{O}(300)$) events have been observed, assuming a 20 (500) GeV dark matter particle. Gen3 xenon experiments can perhaps expect an enhancement in model selection as large as 30% (for the SI this enhancement can be as large as $\simeq 40\%$) for the most optimistic of circumstances, but will still require target complementarity to definitely identify the correct model.

We would like to emphasize that the purpose of this paper is not of a comparison of the SI and anapole interactions, but rather a quantitative assessment of whether time information can be exploited in future direct detection analyses to break degeneracies in the recoil spectrum. The SI and anapole interactions provide one particularly illuminating example of this because they contain different dependencies on the dark matter velocity (and consequently have a different modulation). Despite also having an approximately degenerate recoil spectrum in xenon, the same cannot be said for the SI and SD interactions which have the same dark matter velocity dependence. There do exist, however, other illustrative examples which we briefly consider below.

In Figs. 6 and 7 we consider a comparison of the magnetic dipole and electric dipole interactions for a 125 GeV dark matter particle, assuming a heavy (Fig. 6) and light (Fig. 7) mediator. As before we consider putative detections in future xenon experiments with exposures varying from 2 ton-years to 40 ton-years. The results are rather similar to the SI and anapole comparison in that Gen3 experiments can expect a $\simeq 20\%$ improvement in model selection when time is included in the analysis, but again necessitate target complementarity to fully differentiate these models.

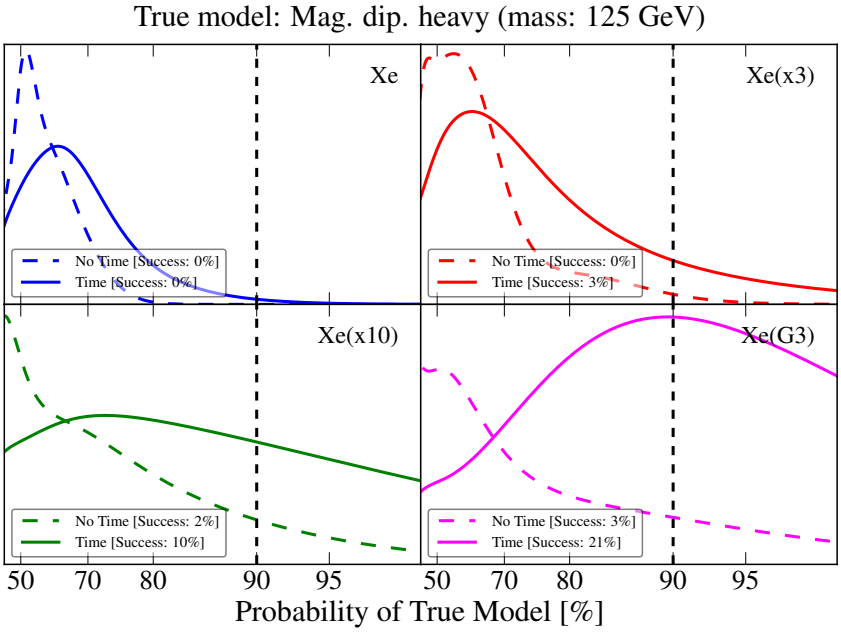

Figure 6. Same as Fig. 3, but now assessing the ability of xenon experiments to break the degeneracy of the magnetic dipole (heavy mediator) and electric dipole (heavy mediator). Results are shown for a 125 GeV dark matter and and assuming the magnetic dipole is the true model.

5 Conclusions

We have considered here the potential impact of using time information in the analysis of future direct detection experiments to break approximate degeneracies that may appear between the recoil spectrum of different interactions. Specifically, we have applied Bayesian model selection to simulated data sets that include the impact of Poisson fluctuations to quantitively assess future ability of xenon experiments to successfully identify approximately degenerate models, assuming analyses include and neglect the time information of detected recoils.

In a comparison of the SI and anapole interactions, we have found that even under the most optimistic of circumstances, including time information in the analysis of Gen2 direct detection does not impact model selection. Rather, correct model identification in Gen2 experiments requires observations in multiple target elements. We have shown that for the inclusion of time information to significantly increase model selection ($\simeq \mathcal{O}(10)\%$) between these two interactions for a single target element, $\simeq \mathcal{O}(1000)$ ($\mathcal{O}(300)$) events must be observed for a 20 (500) GeV dark matter particle. Furthermore, even if time is exploited in Gen3 xenon experiments, target complementarity must also be exploited to unequivocally differentiate these two models.

In addition to the aforementioned example, we have also provided an illustration of this analysis for a comparison of the magnetic dipole and electric dipole interactions. Quantitatively these results are quite similar to those of the SI and anapole interactions.

In the event of a putative signal, future direct detection experiments will be charged with the difficult task of illuminating the high energy behavior of dark matter solely from the observed

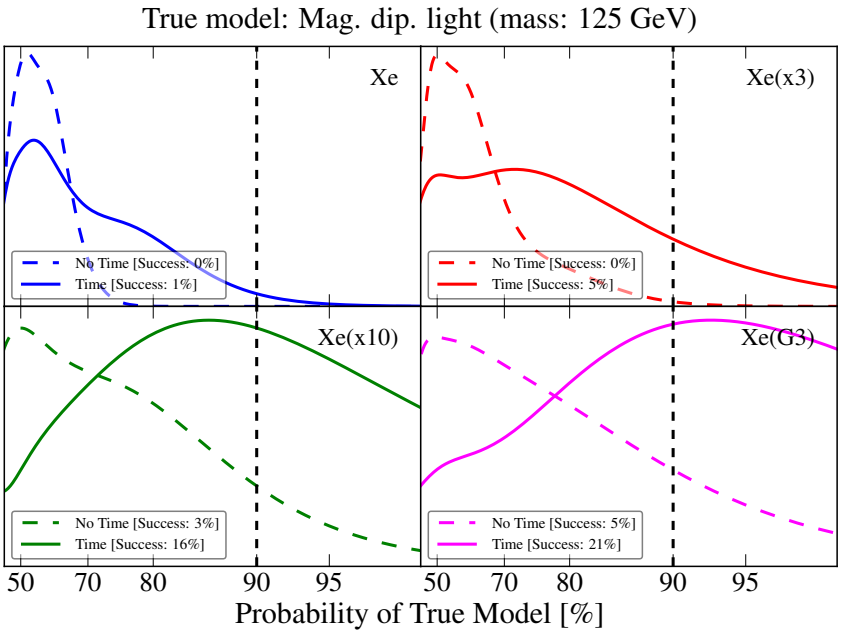

Figure 7. Same as Fig. 6 but for a light mediator.

low energy recoils. This is a particular daunting task in light of the fact that many feasible dark matter models produce nearly degenerate recoil spectra. Exploiting all of the information available, including the time information of nuclear recoils and detections in multiple experiments, will likely be required to make definitive statements regarding the true nature of dark matter.

Acknowledgments. SW is supported under the University Research Association (URA) Visiting Scholars Award Program, and by a UCLA Dissertation Year Fellowship.

A Model Selection Prospects in Xenon (SI Interaction)

We present in Figs. 8-10 the model selection prospects for various exposure xenon experiments, including (solid) and neglecting (dashed) information on the modulation of the rate, and assuming the SI interaction is the true model. Results are shown for 20 GeV (Fig. 8), 125 GeV (Fig. 9), and 500 GeV (Fig. 10) dark matter. Results are similar to those presented in Sec. 4 for the anapole interaction.

References

[1] Snowmass 2013 Cosmic Frontier Working Groups 14 collaboration, D. Bauer et al., *Dark Matter in the Coming Decade: Complementary Paths to Discovery and Beyond*, *Phys. Dark Univ.* **7-8** (2015) 16–23, [1305.1605].

[2] XENON collaboration, E. Aprile et al., *Physics reach of the XENON1T dark matter experiment*, *JCAP* **1604** (2016) 027, [1512.07501].

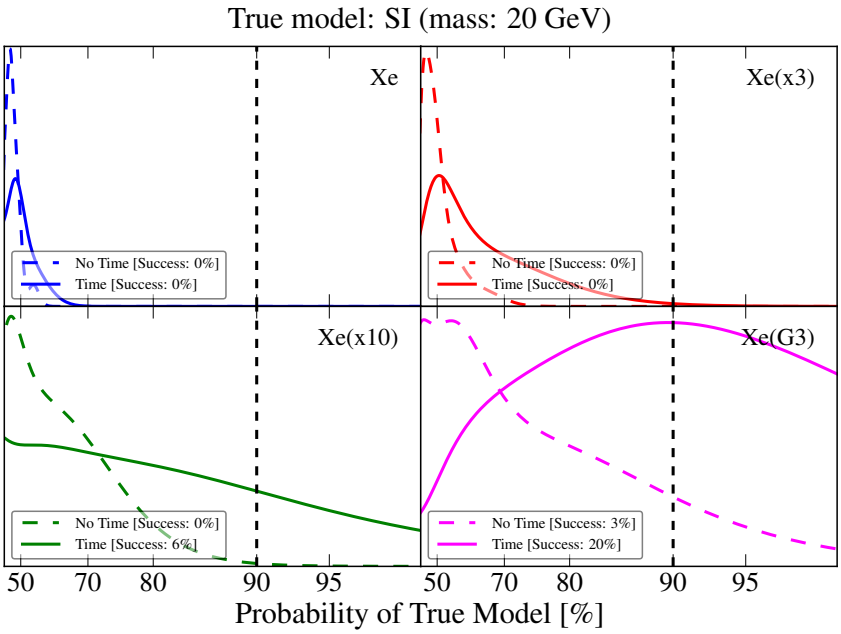

Figure 8. Same as Fig. 3 but for the SI interaction.

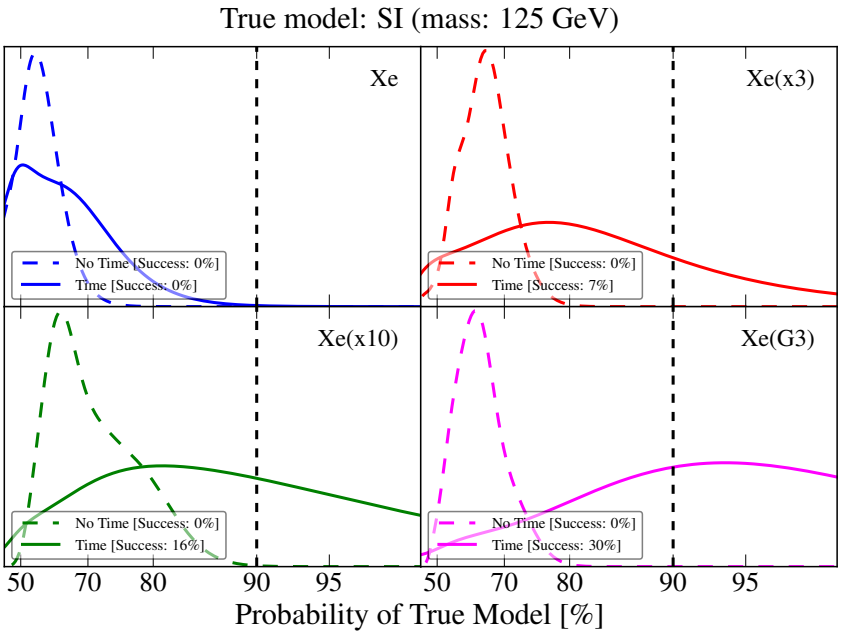

Figure 9. Same as Fig. 3 but for a 125 GeV dark matter and the SI interaction.

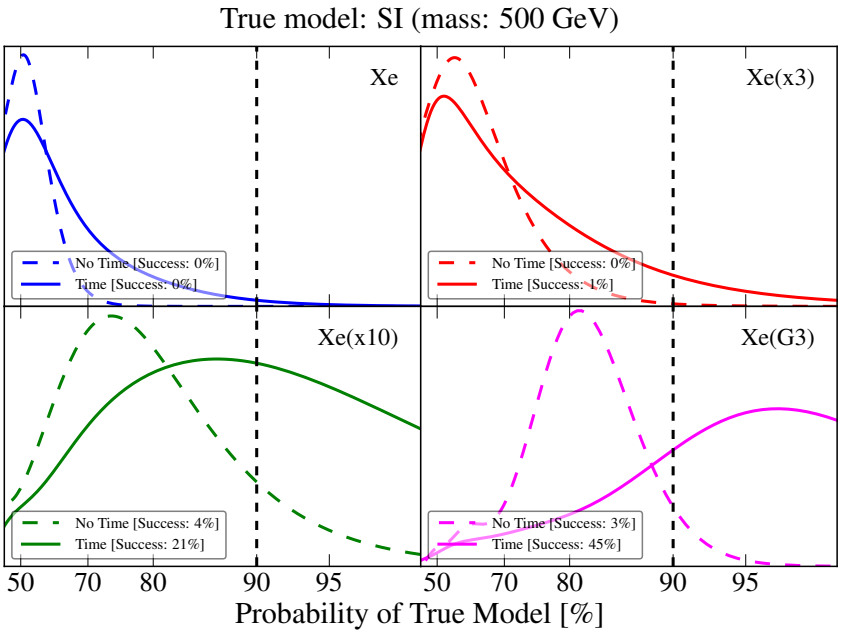

Figure 10. Same as Fig. 3 but for a 500 GeV dark matter and the SI interaction.

[3] SuperCDMS collaboration, R. Agnese et al., *Projected Sensitivity of the SuperCDMS SNOLAB experiment*, *Submitted to: Phys. Rev. D* (2016) , [1610.00006].

[4] D. C. Malling et al., *After LUX: The LZ Program*, 1110.0103.

[5] J. L. Newstead, T. D. Jacques, L. M. Krauss, J. B. Dent and F. Ferrer, *Scientific reach of multiton-scale dark matter direct detection experiments*, *Phys. Rev.* **D88** (2013) 076011, [1306.3244].

[6] P. Cushman et al., *Working Group Report: WIMP Dark Matter Direct Detection*, in *Proceedings, 2013 Community Summer Study on the Future of U.S. Particle Physics: Snowmass on the Mississippi (CSS2013): Minneapolis, MN, USA, July 29-August 6, 2013*, 2013. 1310.8327.

[7] J. Billard, L. Strigari and E. Figueroa-Feliciano, *Implication of neutrino backgrounds on the reach of next generation dark matter direct detection experiments*, *Phys. Rev.* **D89** (2014) 023524, [1307.5458].

[8] F. Ruppin, J. Billard, E. Figueroa-Feliciano and L. Strigari, *Complementarity of dark matter detectors in light of the neutrino background*, *Phys. Rev.* **D90** (2014) 083510, [1408.3581].

[9] J. H. Davis, *Dark Matter vs. Neutrinos: The effect of astrophysical uncertainties and timing information on the neutrino floor*, *JCAP* **1503** (2015) 012, [1412.1475].

[10] J. B. Dent, B. Dutta, J. L. Newstead and L. E. Strigari, *Effective field theory treatment of the neutrino background in direct dark matter detection experiments*, *Phys. Rev.* **D93** (2016) 075018, [1602.05300].

[11] R. J. Hill and M. P. Solon, *Universal behavior in the scattering of heavy, weakly interacting dark matter on nuclear targets*, *Phys. Lett.* **B707** (2012) 539–545, [1111.0016].

[12] R. J. Hill and M. P. Solon, *WIMP-nucleon scattering with heavy WIMP effective theory*, *Phys. Rev. Lett.* **112** (2014) 211602, [1309.4092].

[13] R. J. Hill and M. P. Solon, *Standard Model anatomy of WIMP dark matter direct detection II: QCD analysis and hadronic matrix elements*, *Phys. Rev.* **D91** (2015) 043505, [1409.8290].

[14] A. Berlin, D. S. Robertson, M. P. Solon and K. M. Zurek, *The Bino Variations: Effective Field Theory Methods for Dark Matter Direct Detection*, 1511.05964.

[15] S. Ipek, D. McKeen and A. E. Nelson, *A Renormalizable Model for the Galactic Center Gamma Ray Excess from Dark Matter Annihilation*, *Phys. Rev.* **D90** (2014) 055021, [1404.3716].

[16] S. D. McDermott, *Lining up the Galactic Center Gamma-Ray Excess*, *Phys. Dark Univ.* **7-8** (2014) 12–15, [1406.6408].

[17] T. Appelquist et al., *Stealth Dark Matter: Dark scalar baryons through the Higgs portal*, *Phys. Rev.* **D92** (2015) 075030, [1503.04203].

[18] T. Appelquist et al., *Detecting Stealth Dark Matter Directly through Electromagnetic Polarizability*, *Phys. Rev. Lett.* **115** (2015) 171803, [1503.04205].

[19] A. L. Fitzpatrick, W. Haxton, E. Katz, N. Lubbers and Y. Xu, *The Effective Field Theory of Dark Matter Direct Detection*, *JCAP* **1302** (2013) 004, [1203.3542].

[20] N. Anand, A. L. Fitzpatrick and W. C. Haxton, *Weakly interacting massive particle-nucleus elastic scattering response*, *Phys. Rev.* **C89** (2014) 065501, [1308.6288].

[21] M. I. Gresham and K. M. Zurek, *Effect of nuclear response functions in dark matter direct detection*, *Phys. Rev.* **D89** (2014) 123521, [1401.3739].

[22] V. Gluscevic, M. I. Gresham, S. D. McDermott, A. H. G. Peter and K. M. Zurek, *Identifying the Theory of Dark Matter with Direct Detection*, *JCAP* **1512** (2015) 057, [1506.04454].

[23] S. D. McDermott, H.-B. Yu and K. M. Zurek, *The Dark Matter Inverse Problem: Extracting Particle Physics from Scattering Events*, *Phys. Rev.* **D85** (2012) 123507, [1110.4281].

[24] A. H. G. Peter, V. Gluscevic, A. M. Green, B. J. Kavanagh and S. K. Lee, *WIMP physics with ensembles of direct-detection experiments*, *Phys. Dark Univ.* **5-6** (2014) 45–74, [1310.7039].

[25] V. Gluscevic and A. H. G. Peter, *Understanding WIMP-baryon interactions with direct detection: A Roadmap*, *JCAP* **1409** (2014) 040, [1406.7008].

[26] R. Catena, *Prospects for direct detection of dark matter in an effective theory approach*, *JCAP* **1407** (2014) 055, [1406.0524].

[27] R. Catena, *Analysis of the theoretical bias in dark matter direct detection*, *JCAP* **1409** (2014) 049, [1407.0127].

[28] J. B. Dent, L. M. Krauss, J. L. Newstead and S. Sabharwal, *General analysis of direct dark matter detection: From microphysics to observational signatures*, *Phys. Rev.* **D92** (2015) 063515, [1505.03117].

[29] K. Freese, J. A. Frieman and A. Gould, *Signal Modulation in Cold Dark Matter Detection*, *Phys. Rev.* **D37** (1988) 3388–3405.

[30] K. Freese, M. Lisanti and C. Savage, *Colloquium: Annual modulation of dark matter*, *Rev. Mod. Phys.* **85** (2013) 1561–1581, [1209.3339].

[31] S. K. Lee, M. Lisanti and B. R. Safdi, *Dark-Matter Harmonics Beyond Annual Modulation*, *JCAP* **1311** (2013) 033, [1307.5323].

[32] V. Britto and J. Meyers, *Monthly Modulation in Dark Matter Direct-Detection Experiments*, *JCAP* **1511** (2015) 006, [1409.2858].

[33] E. Del Nobile, G. B. Gelmini and S. J. Witte, *Gravitational Focusing and Substructure Effects on the Rate Modulation in Direct Dark Matter Searches*, *JCAP* **1508** (2015) 041, [1505.07538].

[34] C. Kouvaris and N. G. Nielsen, *Daily modulation and gravitational focusing in direct dark matter search experiments*, *Phys. Rev.* **D92** (2015) 075016, [1505.02615].

[35] E. Del Nobile, G. B. Gelmini and S. J. Witte, *Target dependence of the annual modulation in direct dark matter searches*, *Phys. Rev.* **D91** (2015) 121302, [1504.06772].

[36] E. Del Nobile, G. B. Gelmini and S. J. Witte, *Prospects for detection of target-dependent annual modulation in direct dark matter searches*, *JCAP* **1602** (2016) 009, [1512.03961].

[37] J. Bovy and H.-W. Rix, *A Direct Dynamical Measurement of the Milky Way's Disk Surface Density Profile, Disk Scale Length, and Dark Matter Profile at 4 kpc $\lesssim R \lesssim$ 9 kpc*, *Astrophys. J.* **779** (2013) 115, [1309.0809].

[38] T. Piffl et al., *The RAVE survey: the Galactic escape speed and the mass of the Milky Way*, *Astron. Astrophys.* **562** (2014) A91, [1309.4293].

[39] J. M. A. Danby and G. L. Camm, *Statistical dynamics and accretion*, *Monthly Notices of the Royal Astronomical Society* **117** (1957) 50–71, [http://mnras.oxfordjournals.org/content/117/1/50.full.pdf+html].

[40] K. Griest, *Effect of the Sun's Gravity on the Distribution and Detection of Dark Matter Near the Earth*, *Phys. Rev.* **D37** (1988) 2703.

[41] P. Sikivie and S. Wick, *Solar wakes of dark matter flows*, *Phys. Rev.* **D66** (2002) 023504, [astro-ph/0203448].

[42] M. S. Alenazi and P. Gondolo, *Phase-space distribution of unbound dark matter near the Sun*, *Phys. Rev.* **D74** (2006) 083518, [astro-ph/0608390].

[43] D. S. Akerib et al., *Results from a search for dark matter in the complete LUX exposure*, 1608.07648.

[44] S. K. Lee, M. Lisanti, A. H. G. Peter and B. R. Safdi, *Effect of Gravitational Focusing on Annual Modulation in Dark-Matter Direct-Detection Experiments*, *Phys. Rev. Lett.* **112** (2014) 011301, [1308.1953].

[45] J. Bagnasco, M. Dine and S. D. Thomas, *Detecting technibaryon dark matter*, *Phys. Lett.* **B320** (1994) 99–104, [hep-ph/9310290].

[46] N. Weiner and I. Yavin, *UV completions of magnetic inelastic and Rayleigh dark matter for the Fermi Line(s)*, *Phys. Rev.* **D87** (2013) 023523, [1209.1093].

[47] PandaX-II collaboration, A. Tan et al., *Dark Matter Results from First 98.7 Days of Data from the PandaX-II Experiment*, *Phys. Rev. Lett.* **117** (2016) 121303, [1607.07400].

[48] Buchner, J., Georgakakis, A., Nandra, K., Hsu, L., Rangel, C., Brightman, M. et al., *X-ray spectral modelling of the agn obscuring region in the cdfs: Bayesian model selection and catalogue*, *A&A* **564** (2014) A125.

[49] F. Feroz, M. P. Hobson and M. Bridges, *MultiNest: an efficient and robust Bayesian inference tool for cosmology and particle physics*, *Mon. Not. Roy. Astron. Soc.* **398** (2009) 1601–1614, [0809.3437].